# Effect of Jet-Exhaust Streams on Structure of Vortex Wakes

Vernon J. Rossow*
NASA Ames Research Center, Moffett Field, CA 94035
and
Anthony P. Brown†
National Research Council of Canada, Uplands, Ottawa, Ontario, Canada KIA OR6

**The study reported here was initiated by observations of condensation trails that occur behind transport aircraft at cruise altitudes under certain atmospheric conditions. The objective of the study reported is to explain why the structure of condensation trails behind aircraft at cruise altitudes differ in some respects from those predicted by classical theory for the roll-up of lift-generated vortex sheets. Because classical roll-up theory does not include the effect of jet-engine exhaust on wake structure, numerical simulations were carried out for the time-dependent interaction of jet-exhaust streams with lift-generated vortex distributions. The simulations indicate that inclusion of jet-exhaust effects produces results that more closely represent observed wakes than those calculated by means of classical roll-up theory. In particular, jet-exhaust streams appear to cause wakes to separate into several nearby parts so that the vertical depth of the wake is increased by over a factor of two. It is therefore recommended that wake-prediction methods include the effect of jet-exhaust streams during takeoff, climb and cruise. Current prediction methods for wake-hazardous regions during approach and landing at airports probably do not need to be changed because engine thrust is small during those operations.**

**Nomenclature**

A = wing planform area , $ft^2$ ($m^2$)
AR = $b^2/A$ = wing aspect ratio
b = wingspan, ft (m)
b' = span-wise distance between vortex centers $\approx \pi b_g/4$, ft (m)
$C_L$ = lift coefficient = $Lift/q_\infty S$
$G_o$ = $\Gamma_o/b_o U_\infty$
Lift = $\rho_\infty U_\infty |\Gamma_o| b'$, lbs (N)
$q_\infty$ = $\rho_\infty U_\infty^2/2$

* Ames Associate, Aviation Systems Division, Mail Stop 210-10, AIAA Associate Fellow.
† Research Scientist, Flight Research Laboratory, Bldg. U-61, Research Road, Ottawa, AIAA Senior Member.

S = planform area of wing, $ft^2$ ($m^2$)
t = time, s
T = $t\Gamma_o/b_o^2$
x = distance in flight or longitudinal direction, ft (m)
X = $x/b_o = T/G_o$
y, z = distance in lateral and vertical directions, ft (m)
u, v, w = velocity components in x, y and z directions, ft/s (m/s)
$U_\infty$ = velocity of wake-generating aircraft, ft/s (m/s)
Wt = weight, lbs (N)
$\gamma$ = $-d\Gamma/dy$
$\Gamma$ = circulation bound in wing, $ft^2$/sec ($m^2$/s)
$\rho$ = air density, slugs/$ft^3$ (kg/$m^3$)

Subscripts
ell = elliptical span-wise loading
fil = vortex filament
g = wake-generating aircraft
lnk = linking of vortex pair
lw = long-wave instability of vortex pair
o = reference quantity
oval = streamline oval that encloses vortex pair
pln = plan view
pr = vortex pair
RTJ = R. T. Jones weight-optimized span loading
$\infty$ = free-stream condition

## I. Introduction

The lift-generated swirling motions in aircraft wakes brought about by the lift-generated trailing vortices are so strong that they usually dominate the organized across-trail velocity components in the wake. For this reason, theoretical and experimental studies of lift-generated vortex wakes have usually not included the effect of jet-exhaust streams on wake structure and on the spread or movement of the hazardous region posed by the vortices in the wake [1-7]. To be sure that such a neglect was tolerable, a study was made of the effect of engine thrust on maximum measured wake-induced rolling moments on aircraft when they encounter the wakes of preceding aircraft [8]. It was found that the measured maximum rolling moments in wakes where jet effects were present are smaller than when the wake-generating aircraft was in its approach configuration and gliding toward a landing. It was also found that the reduction in the maximum measured value for wake hazard brought about by engine thrust was far from

sufficient to render wakes non-hazardous for in-trail penetration. For these reasons, classical roll-up theory was believed to be sufficiently accurate for the estimate of the maximum and the distribution of wake-induced rolling moments in lift-generated wakes of aircraft at cruise altitudes and in the airport environment [3-10].

The study presented here was initiated by the observation that the structure of condensation trails[#] behind aircraft at cruise altitude have features not present in wakes predicted by classical roll-up theory for vortex wakes [1,2,9]. The observations suggest that even though engine thrust does not alleviate wakes enough to render them harmless, the energy content in the jet-exhaust streams from the engines is large enough to produce significant distortions to wake structure through displacement and rearrangement of vortex elements brought about by turbulent mixing with the ambient air and by the deceleration of jet-exhaust streams as they age.

The objective of the present study is to show how jet-engine exhaust streams appear to cause lift-generated vortex wakes to divide and become more complicated than predicted by classical theory. The study reported is directed at the determination of why the visual structure of condensation trails sometimes differs considerably from the structures predicted by classical roll-up theory for lift-generated vortex sheets [5,6]. In order to accomplish these objectives, theoretical and observational information is provided to improve the understanding and prediction capability of the structure of lift-generated wakes of aircraft as they move and spread as a function of time under the influence of its vortex and engine-exhaust flow-field components. Pictures are first presented of condensation trails at cruise altitudes to illustrate the more complex appearance of lift-generated wakes at cruise altitudes where the effect of jet-exhaust streams on their structure is visualized. Classical roll-up theory is described to provide a background for cases wherein the flow-field structure is driven by only the vortex sheet shed by the wing, so that they do not separate into several parts that substantially increase wake size. Point-vortex and point-source representations along are then used to simulate the time-dependent motion of wakes at cruise altitudes in order to illustrate and explain some of the details of the interaction of vortex wakes and engine exhaust streams. It is assumed that the fluid motions studied can be treated by use of inviscid and incompressible flow theory.

[#] Condensation trails appear behind aircraft when they fly at cruise altitudes, because the atmosphere at those altitudes is often at temperatures below -40$^{o}$F (or -40$^{o}$C), and a relative humidity above 40%. These conditions cause the water vapor in engine exhaust gases to condense and freeze into ice crystals before they have time to evaporate

## II. Observations of Dynamics of Condensation Wakes.

The photographs presented in Fig. 1 are part of a larger set taken at long range from the ground in order to study how the structure of vortex wakes at cruise altitudes changes with time, and how rapidly the hazardous parts of wakes spread as a function of time [1]. At the time of the photographs, conditions at cruise altitudes were such that condensation and freezing of water vapor in engine exhaust products visualized the complete wake, and not just the high-speed vortex-core regions of the vortices [3,4]. The photograph in Fig. 1a presents a side view of the beginning segment of a condensation trail behind an aircraft before any wake structure becomes prominent enough to be discernable. About one-half minute after passage of the wake-generating aircraft, Fig. 1b, the condensation trail has changed from being quite small to one where the condensation appears to have separated into an upper and lower part, and the long-wave instability [3,4] has begun to grow. The sinuous waves associated with the long-wave instability are prominent in the lower part of the condensate as dense tubes of condensation. The tube-like formations are robust regions that form at the high-speed centers of rolled-up vortex sheets. As time progresses, the amplitude of the along-axis waves on the filaments become larger and more prominent until the vortices link across the centerline of the wake near the bottom of the condensate; Figs. 1b and 1c. When linking occurs, the initial single and rather small condensate-marked region shown on the left side of Fig. 1a has

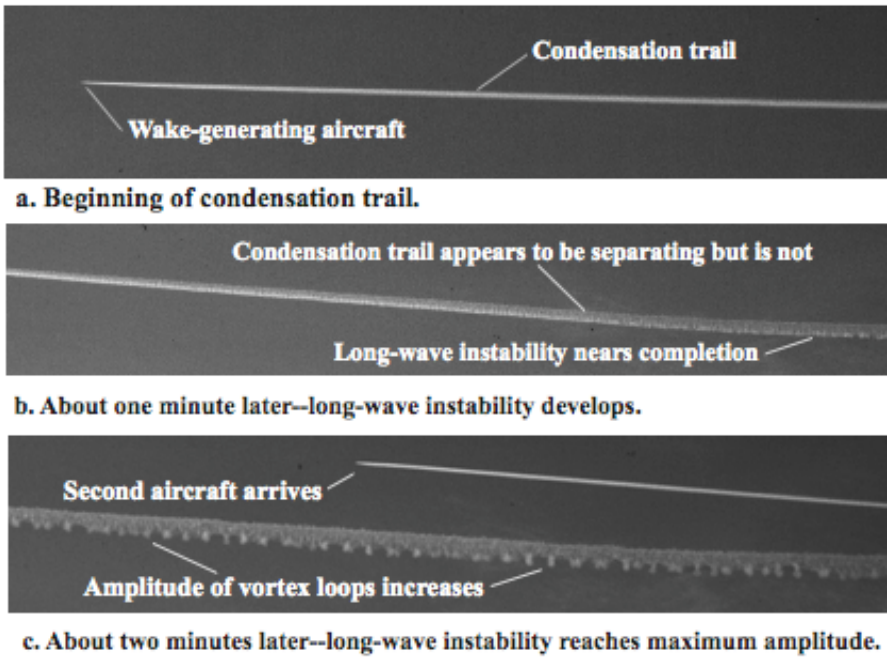


Fig.1 Time history of decomposition of lift-generated wakes as visualized by condensation of exhaust gases in stream from jet engines.

or sublime. Under those conditions, exhaust condensate becomes a fluid marker of long duration that makes it possible to observe the dynamics of lift-generated vortex wakes over a wide range of conditions.

grown by about a factor of five or more by mixing with the atmosphere and by sinuous mixing brought about in the wake by the long-wave instability as shown in Fig. 1c. It is also noted that the condensate first becomes most dense in the lower part of the wake (middle of Fig. 1b), and then becomes most dense in the upper part of the wake above where the long-wave instability has occurred; Fig. 1c. This change is believed to be brought about by the circulatory flow field of the vortex pair that tends to move condensate from the bottom of the wake to the top of it. Analysis of a large number of observations indicate that condensation trails spread roughly as the square root of time during their visual existence [1].

An example of complete wake separation is shown in Fig. 2. The picture was taken from an aircraft flying beside and into the wake of another aircraft to make measurements of wake velocities [2]. The objective of the flight tests was to evaluate potential hazards to aircraft that might accidentally penetrate a lift-generated wake. In the photograph, the formation of two distinct regions of wake fluid indicate that the wake has, in this case, divided into two parts that probably continue to aerodynamically communicate with each other. The lower part of the

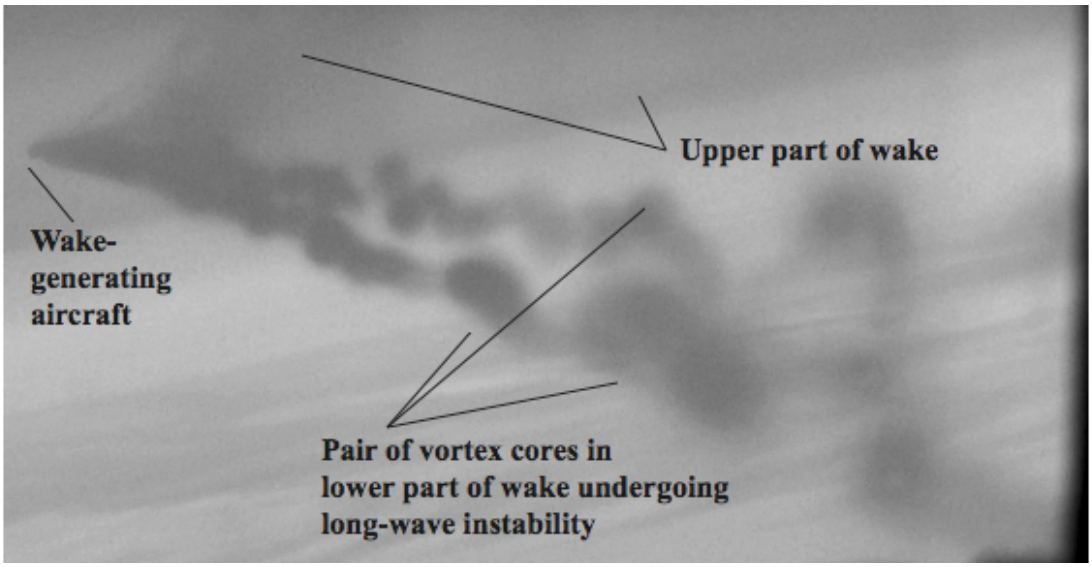


Fig. 2 Photograph taken from nearby aircraft of the condensation trail of a transport aircraft at cruise altitude. View along wake from behind shows wake separation into upper and lower parts. Upper part appears to not contain a pair of concentrated vortex cores, whereas lower part does contain a pair of intense vortex cores that are undergoing the long-wave instability [2-4].

condensation trail contains a pair of vortex filaments clearly marked by condensation where the vortex pair is going through the development of the long-wave instability [3,4]. The upper part appears to be a cloud of condensate without any organized structure or presence of an organized

vortex pair. Also, a non-condensate vertical distance exists between the two parts of the wake. The upper region is some times referred to as the jet-wake part of the condensation trail, because it appears to consist primarily of engine exhaust, and the lower region as the vortex wake, because a pair of vortex cores undergoing the long-wave instability is prominent in that part of the wake.

The foregoing photographs are typical of a number of cases observed in which condensation trails appear to divide into upper and lower parts that remain in touch with or near to each other during the lifetime of the wake. Not apparent in these photographs, but clear in enlarged views, is that the upper region does not exhibit any dominant vortex-like structures, but appears to be composed primarily of a large-scale turbulent flow field with eddies as large as or larger than the wing span of the wake-generating aircraft. The lower region appears to consist primarily of a pair of vortices that undergo the long-wave instability [1-4], and large turbulent eddies are not observed. As the vortex pair executes the wake dynamics associated with the long-wave instability, the amplitude of the waves on the filaments at the bottom of the condensate cloud becomes large enough to dominate wake motions, especially in the lower part of the trail. During this time, the upper part of the wake becomes larger because of turbulent mixing and because the condensate has accumulated there by convection of the velocity field of the vortex pair; Fig. 1c.

## III. Classical Roll-Up of Vortex Sheets.

The idealized or classical roll-up of vortex sheets shed by aircraft wings is presented to describe

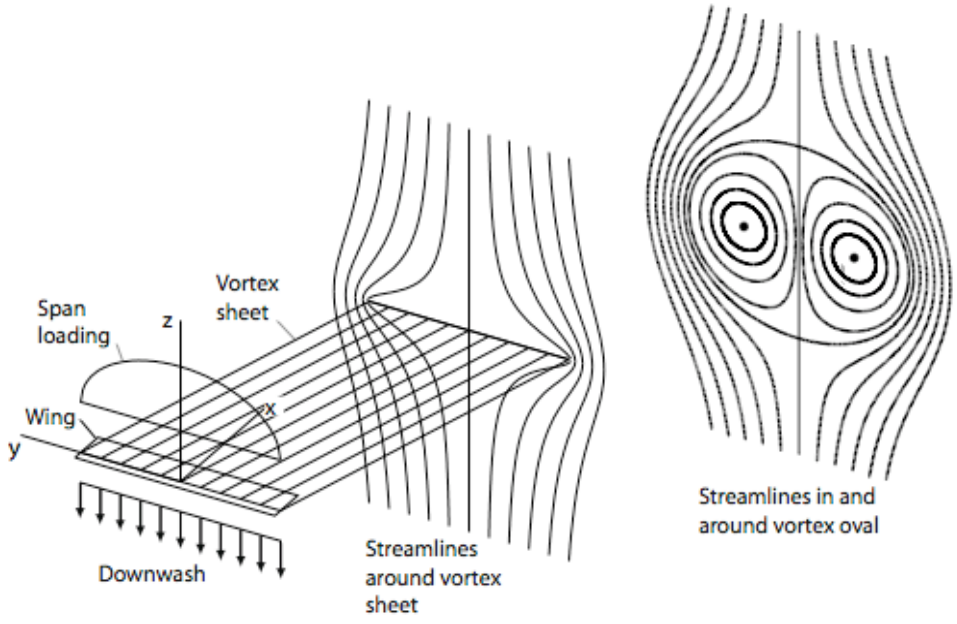


Fig. 3 Oblique view of idealized theoretical model of roll up of vortex sheet shed by elliptically loaded wing into vortex oval [9].

the way that the structure of lift-generated vortex wakes have usually been estimated in the past [9]. Based on the span loading on the wake-generating wingand the model shown in Fig. 3, the magnitude of the swirl velocity distribution in the vortices can be accurately predicted [5,10]. The prediction process assumes that the vortex sheet generated by the lift on the wing of the aircraft begins at z=0 and the x=0 station where the quarter chord of the wing is assumed to be located. Classical theory for roll-up of vortex sheets, Fig. 3, assumes that the upward component of the flow of the free stream around the wing is given by $U_\infty \sin\alpha = w_\infty$ , where $\alpha$ is the angle of attack of the wing relative to zero lift for an elliptically loaded wing. The circulation bound in the wing is related to the span loading by

$$\gamma(y,0) = -d\Gamma(y,0)/dy \qquad (1)$$

The vortex sheet is assumed to initially be flat, and of zero thickness so that it has zero cross-sectional area. When the vortex sheet rolls up continuously from its two side edges, it forms two well-organized vortices of opposite sign, as shown in Fig. 3, the roll-up process envelops and encloses a quantity of fluid to form an elliptically-shaped oval (the vortex oval) that has a finite cross-sectional area and travels downward with time. When the span loading on the wing is not elliptic, the structure of the vortex pair inside the oval still depends on the span loading on the wake-generating wing, and can therefore be estimated theoretically [5,10]. The cross-sectional area associated with the vortex pair, when it is rolled up, is then a consequence of inviscid fluid dynamics and not a result of exhaust entrainment or turbulent mixing.

Another theoretical model must and will be used to analyze the more complex flow fields associated with the development of lift-generated flow fields when jet-exhaust streams are present. The numerical method used to compute the more realistic flow fields to be presented also includes roll-up entrainment, but uses point-vortex elements to simulate the actions of the circulation in the shed wake, and point-source elements to simulate exhaust jet-streams to simulate deceleration, mixing and entrainment of jet-exhaust streams with ambient air. Other numerical examples of the time-dependent roll-up of vortex wakes are presented after the method used has been described.

## IV. Trefftz-Plane Analysis of Wake Dynamics.

### A. Overview of Method.

The computational method used to compute the time-dependent dynamics of lift-generated vortex wakes with and without the presence of jet-exhaust gases is made by use of point-vortex and point-source distributions in the so-called Trefftz plane [5,6,11-14]. The simulations begin

immediately behind the aircraft where the initial locations of the singularities are known. The Trefftz-plane approximation simplifies the computations by use of the approximation that wake-induced velocities are most important in the vertical and lateral directions, and negligible in the flight direction, so that their variations from the free-stream velocity can be ignored. The roll-up of vortex sheets can then be treated as a time-dependent, across-stream problem. As a consequence of the assumptions made, the technique does not represent three-dimensional instabilities, like the long-wave instability of a vortex pair [3,4]. It is also assumed that the fluid is incompressible and inviscid.

**B. Span-Wise Loadings Considered.**

Because measured span-wise loadings are not available for the aircraft that generate the condensation trails of interest, realistic estimates are needed as starting points for the computations to be carried out to estimate the observed wake behavior. Two idealized span loadings were chosen for the study because they shed vortex wakes that are representative of two kinds of span-wise loadings designed for aircraft in the past. They are: 1) elliptical span loading, derived by Munk [15,16] as the span loading that has the least lift-induced drag for a given lift and wing span; and, 2) a span loading designed by R. T. Jones [17] as the span loading that has the least lift-induced drag for a given lift and given minimum wing-root bending moment (i.e., least structural weight) (Fig. 4). The Jones-optimized design, RTJopt, is a combination of triangular and elliptical downwash distributions along the span of the wing.

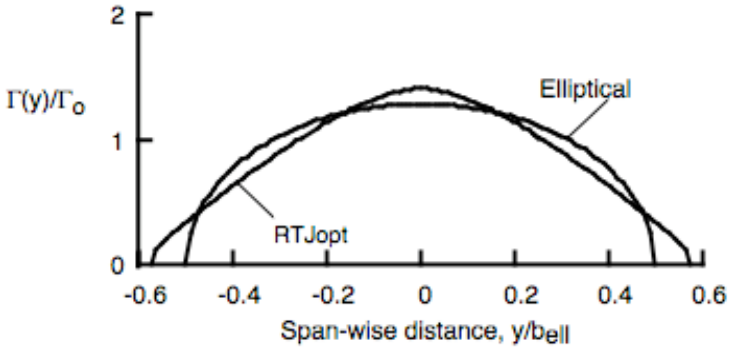

Fig. 4 Span loadings on isolated wings to be used as basis for study of wakes. Total lift by each lifting distribution is the same so that Lift = $\rho U_\infty |\Gamma_o| b_o$ .

Although current designs resemble the span loading proposed by Jones, an exact match is not likely because high-speed computers are used to optimize the design of not only the wings, but also of the entire structure of the aircraft. In that way, interactions of the various components of the aircraft with each other are included in the computations used to optimize the design. As a result, the numerical solutions obtained for the span-wise loadings of lift on subsonic transports

are no longer accurately represented by simple functions like those obtained by Munk and Jones. The Munk design [15,16] was chosen because it sheds a vortex sheet with circulation concentrated at the wingtip region, whereas the Jones design sheds circulation much more uniformly distributed along the span.

An elliptically loaded wing has a span-wise loading given by

$$\Gamma_{ell}(y)/\Gamma_o = (4/\pi)[1 - (2y/b_o)^2]^{1/2} \qquad (2)$$

where, $\Gamma_{ell}(y)$ is the span-wise distribution of circulation bound in the wing to represent the lift on an elliptically loaded wing of span $b_o$ that carries the same total lift, lift = $\rho|\Gamma_o|b_o U_\infty$, as a wing with uniform loading, $\Gamma_o$, and a span of $b_o$. The second span loading to be used in the study is one of the family of designs produced by R. T. Jones [17]. Each span-wise loading is optimized for minimum induced drag for a given lift, span and wing-root bending moment. Each wing-span used in the design then has a particular combination of a uniform and a triangular down-wash distributions at the trailing edge of the wing, which makes it more complex than the elliptic distribution. The span loading used here is written in closed form as

$$\Gamma_{RTJ}(y)/\Gamma_o = [(12/\pi + 6\,Yp)/(b_{RTJ}/b_o)]\,[1 - (2y/b_{RTJ})^2]^{1/2} + \{(18Yp - 24/\pi)(4y^2/b_{RTJ}^2)\ln[(b_{RTJ}/2y) + ((b_{RTJ}/2y)^2]^{1/2}\}/(b_{RTJ}/2y) \qquad (2)$$

where $b_{RTJ}/b_o = 1.15$ is the particular span ratio recommended by Jones [17] as most practical and assumed for the weight-optimized design used in the present study. The quantity $\Gamma_{RTJ}(y)$ is the span-wise distribution of bound circulation in the wing. The quantity Yp is defined as $Yp = 4b_o/(3\pi b_{RTJ})$.

**C. Computational Method.**

The initial span-wise distribution of circulation in the vortex sheet shed by the wing at the moment the aircraft passes through a vertical plane at the trailing edge of the wing yields the initial distribution of vorticity in the vortex sheet as,

$$\gamma(y,0) = -d\Gamma(y,0)/dy \qquad (3)$$

where, $\Gamma(y,0)$ is the magnitude of the bound circulation in the wing as a function of span-wise distance. The beginning structure of the vortex sheet is used as the initial conditions for the subsequent time-dependent motion of segments of the vortex sheet. Segments of the vortex sheet are obtained by dividing the vortex sheet into span-wise segments of equal length so that the vortices are equally spaced, but they do not all have the same circulation content. The centers of the point vortices are located at the centers of the segments of vortex sheet they represent, which results in a step-wise representation of the span-wise variation in the circulation bound in the wing and of the strength of the vortex sheet shed at the trailing edge of the wing. The time-wise development of the vortex sheet in the plane where the computations are being made moves away from the trailing-edge of the wake-generating aircraft at the flight velocity, $U_\infty$, so that it remains with the same body of fluid during the event. In this way, the two-dimensioanl time-dependent computations produce a representation of the three-dimensional structure of the wake.

For the general case, the span-wise or lateral and vertical velocity components for the ith point vortex, as induced by a summation of the contributions of each jth point vortex are given by [5,6,11-13]

$$v_i = - (1/2\pi) \sum_{j=1}^{N} \gamma_j[(z_i - z_j)]/[(y_i - y_j)^2+(z_i - z_j)^2] \tag{4a}$$

$$w_i = +(1/2\pi) \sum_{j=1}^{N} \gamma_j[(y_i - y_j)]/[(y_i - y_j)^2+(z_i - z_j)^2] \tag{4b}$$

where, N is the number of point vortices used to represent the sub-divided vortex sheet, $\gamma_j$ is the circulation content of the jth point vortex, and $v_i$ and $w_i$ are the lateral and vertical velocity components of the ith vortex. The velocity, $u_i$, in the flight or x-direction of the various point vortices (sheet segments), is assumed to be $U_\infty$ relative to the aircraft, and stationary relative to the ambient air. In a flight situation, the along-axis movement of the vortex elements is in the same direction as the jet-engine exhaust, but is not as rapid. The influence of the jet streams first stretches the vortex cores, and then compresses them as the jet-exhaust streams decelerate. As the wake ages, the component of the velocities of the jet exhaust and vortex cores in the flight direction both tend toward zero relative to the ambient air. The effect of first being stretched and then compressed on vortex dynamics is assumed to be small, and is therefore ignored in the present study.

In certain cases, the distribution of vorticity in the vortex sheet can be assumed to be perfectly symmetrical or anti-symmetrical about the centerline of the wake. For anti-symmetrical vortex wakes, which is the wing case, computational time can be saved by writing Eqs. (4) for the anti-symmetrical case as

$$v_i = -(1/2\pi) \sum_{j=1}^{N} \gamma_j \{[(z_i - z_j)]/[(y_i - y_j)^2+(z_i - z_j)^2] - [(z_i - z_j)]/[(y_i + y_j)^2+(z_i - z_j)^2]\} \qquad (5a)$$

$$w_i = +(1/2\pi) \sum_{j=1}^{N} \gamma_j \{[(y_i - y_j)]/[(y_i - y_j)^2+(z_i - z_j)^2] - [(y_i + y_j)]/[(y_i + y_j)^2+(z_i - z_j)^2]\} \qquad (5b)$$

where, $v_i = dy_i/dt$ and $w_i = dz_i/dt$ relate the magnitude of the velocity components to the changes in the time-dependent locations of the point vortices, $(y_i,z_i)$. Equations (5) insure perfect anti-symmetry of motion and save some computational time. Because the wakes are assumed to be perfectly anti-symmetrical, the quantity N is taken as the number of point vortices on one side of the wake, and not the total number of vortices in the flow field, 2N.

In the integration for the time-dependent locations of the vortices, accumulation of computational errors are minimized by use of several techniques. First, the choice of the size of the maximum amount of circulation in each point vortex is controlled by the number of point vortices chosen to represent the vortex wake. The size of the time step, and the number of iterations on vortex motion, are also chosen by trial and error to be a size that makes the motion of the vortices orderly. In addition, when two vortices approach each other too closely, each point vortex is assumed to have a vortex core structure wherein the magnitude of the swirl velocity decreases linearly from that given by Eqs. (4) and (5) to zero at the center of the point vortex. The core radius is set equal to four initial spacings between the vortices. Therefore, when two vortices approach each other within a distance less than the chosen core radius, the swirl velocity magnitude induced by one vortex on another in the array is softened so that erratic vortex motions are suppressed. The lateral and vertical velocities induced on vortices in the array are then given by

$$v_i = -(1/2\pi) \sum_{j=1}^{N} \gamma_j \{[(z_i - z_j)]/[r_c^2] - [(z_i - z_j)]/[(y_i + y_j)^2+(z_i - z_j)^2]\} \qquad (6a)$$

$$w_i = +(1/2\pi)\sum_{j=1}^{N} \gamma_j\{[(y_i - y_j)]/[r_c^2] - [(y_i + y_j)]/[(y_i + y_j)^2+(z_i - z_j)^2]\} \quad (6b)$$

where, $r_c$ is the core radius (solid body rotation) given to each vortex structure. Eqs. (5) are used when the distance between the ith and jth vortices, $[(y_i - y_j)^2+(z_i - z_j)^2]$, is greater than or equal to $r_c$, and Eqs. (6) are used when the distance between the two vortices is less than $r_c$. These relationships help to prevent unrealistic excursions of point vortices whenever they pass closely to each other, and tend to assist in the formation of vortex cores, rather than dispersing them.

The foregoing equations are made dimensionless by dividing the lateral $v_i$ and vertical $w_i$ velocity components by the flight velocity, $U_\infty$, of the wing through the atmosphere. In the computations, the time is made dimensionless by a grouping of parameters as $T = t\,\Gamma_o/b_o^2$. The various quantities are also related to one another through the lift on the wing as

$$\text{Lift} = \rho U_\infty |\Gamma_o| b_o \quad (7)$$

The time parameter is also related to the self-induced downward velocity of the vortex wake given by

$$w_{pr} = |\Gamma_o|/2\pi b'_o \quad (8)$$

where $b'_o = b_o\pi/4$ and $\Gamma_o/b_oU_\infty = 2C_{Lg}/\pi AR_g$. Because $C_{Lg} \approx 1.0$ during cruise flight, and $AR_g \approx 7$ for subsonic transports, the distance in span lengths, $x/b_o$, behind the wake-generating aircraft is related to the computational time by

$$X(T) = x(t)/b_o = t\,U_\infty/b_o = T/(\Gamma_o/b_oU_\infty) = T/G_o \quad (9)$$

where $G_o = \Gamma_o/b_oU_\infty$ is around 0.1 to 0.2. In the figures to follow, $G_o$ will be assumed to be 0.2 for simplicity, and for compactness. The distance behind the wake-generating aircraft is then related to the dimensionless time by

$$x/b_o \approx 10\,T \quad (10)$$

## V. Motion of Point-Vortex Representations.

**A. End Views of Wake Dynamics.**

By use of the computational method described previously, rear views of the point-vortex representations of the two vortex wakes being studied are presented in Figs. 5 and 6 at several different times during the early part of the roll-up process. The vortex sheet shed by the elliptic span-loading model is divided into 20 point vortices per side (40 point vortices total). Because the span of the wing used for the R. T. Jones loading is 1.15 times larger than the one used for elliptic loading, its vortex sheet was divided into 23 segments (46 point vortices total). The larger number of segments is required so that the spacing between vortices is the same for both models, as is the total lift.

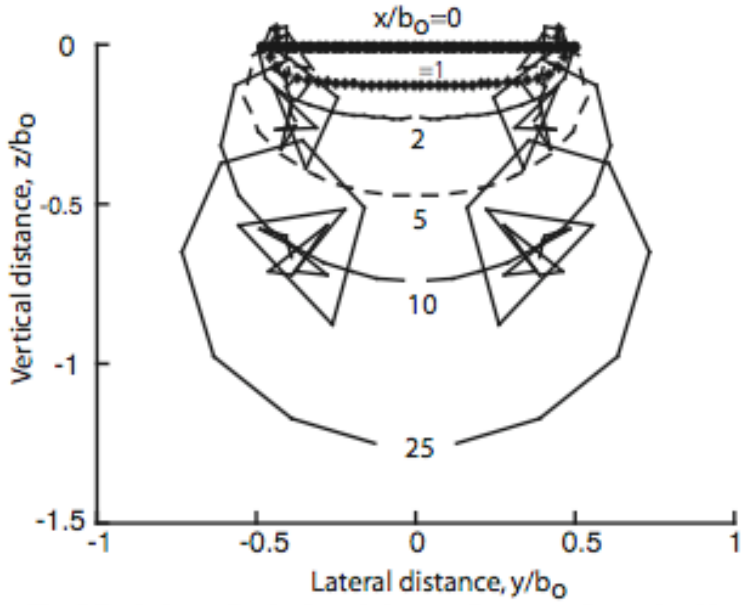


Fig. 5 End view of calculated shape of vortex sheet shed by wing with elliptic span loading during early part of roll-up process.

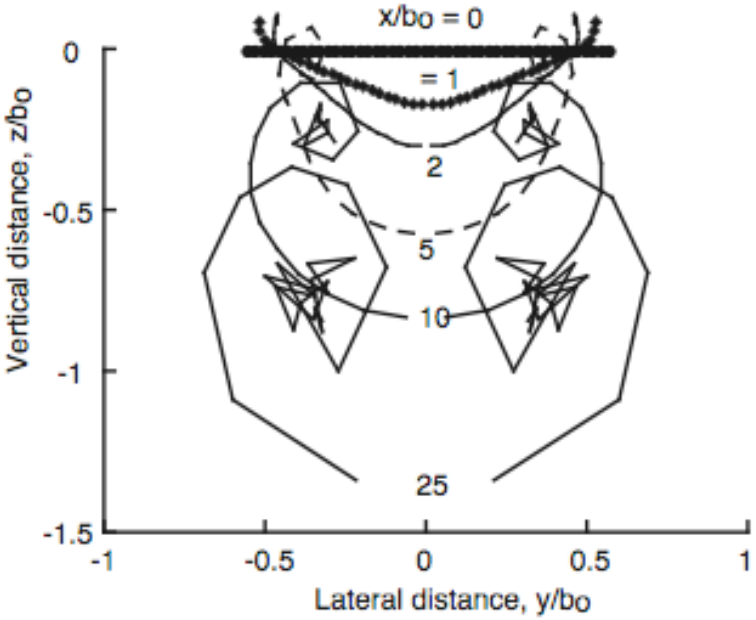


Fig. 6 Calculated shape of vortex sheet shed by R.T. Jones span loading during early part of roll-up process.

Elliptic span loading is studied first, because it is the most familiar of those used to design aircraft wings (Fig. 5). The locations of the point vortices in Figs. 5 and 6 are connected by lines at each downstream station to more clearly identify the shape of the vortex

sheet at a given time. The vortex sheets are assumed to be flat at the beginning of each event. Roll up of each sheet as represented by point-vortex distributions indicates the status of the sheet shape as it changes from a flat surface into a pair of fully-developed nearly round vortices. The roll-up process causes the initially flat vortex sheet to envelop enough ambient fluid to fill an elliptically-shaped cross-sectional area of over about two spans in width and $3^{1/2}$ in depth. The final vortex oval contains all of the circulation (point vortices) in the wake and moves downward at a velocity given by

$$w_{pr} = - |\Gamma_o|/2\pi b_o' U_\infty \qquad (11)$$

As shown in Fig. 5, the vortex sheet shed by an elliptically-loaded wing first descends at about the same speed all along the span except near the wingtips, where a strong up-wash occurs. In the wingtip region, the up-wash turns into a rotational motion brought about by the nearby vortices. In this way, vortex cores are produced that cause the vortex sheet to roll up from the wingtips inboard to the wake centerline, with somewhat concentrated cores at the two centers of the rollup. The left and right sides of the wake are mirror images of each other.

In the beginning of the roll-up process, the RTJ loading produces a nearly triangular downwash pattern (e.g., $x/b_o$ = 1 and 2) over the outboard part of the wake, and an almost constant downwash over the inboard part of the span. As time progresses, the initial downwash patterns are replaced by the swirling flow fields of vortex pairs. The structure of the two swirling flow fields can be predicted with good accuracy by use of a method derived by Betz [5,6]. After that, the structure of the rolled-up vortices changes very slowly with time until three-dimensional instabilities set in to cause the orderly structure of the vortex pair to decompose. The turbulent motions brought about in the wake by its decomposition cause the lift-generated flow field to spread further by turbulent decay [1].

**B. Side Views of Wake Dynamics.**

Because the observer is usually on the ground and the condensation trails at cruise altitude, observations of wakes are made from a side-ways diagonal view towards the wake. The side views presented in Fig. 7 derived computationally then supplement the computationally derived end views of the wake dynamics shown in Figs. 5 and 6. The numerically-generated lines in the figures represent the paths traveled by the point vortices as a function of downstream distance. The paths of the point vortices approximate vortex filaments as they trail downstream from the

wing for about 100 span lengths (≈ 0.5 minute) of travel. In this way, the figures present the development of the vortex sheet from when it was shed to far downstream behind the wake-generating wings.

Figure 7 displays the changes in wake structure as a function of time during the roll-up process along with the smaller changes that occur at larger distances behind the wing. The figures illustrate how the individual vortex elements orbit about a central core region where the centroids of vorticity (or circulation) are located. The filament motions indicate that wake separations or multiple vortex pairs, do not form for these two configurations. The motion of the two vortex sheets differs most at the beginning of the roll-up process where the time at which the outer-most vortices take longer to be rolled into the vortex structure for elliptic loading than for the RTJ loading. Also, the paths of the vortices for the RTJ loading appear to be more compact than those for elliptic loading. In addition, the larger circulation content and the more inboard loading of the RTJ vortex sheet causes it to descend a bit more rapidly than the vortex sheet shed by an elliptic-loaded wing.

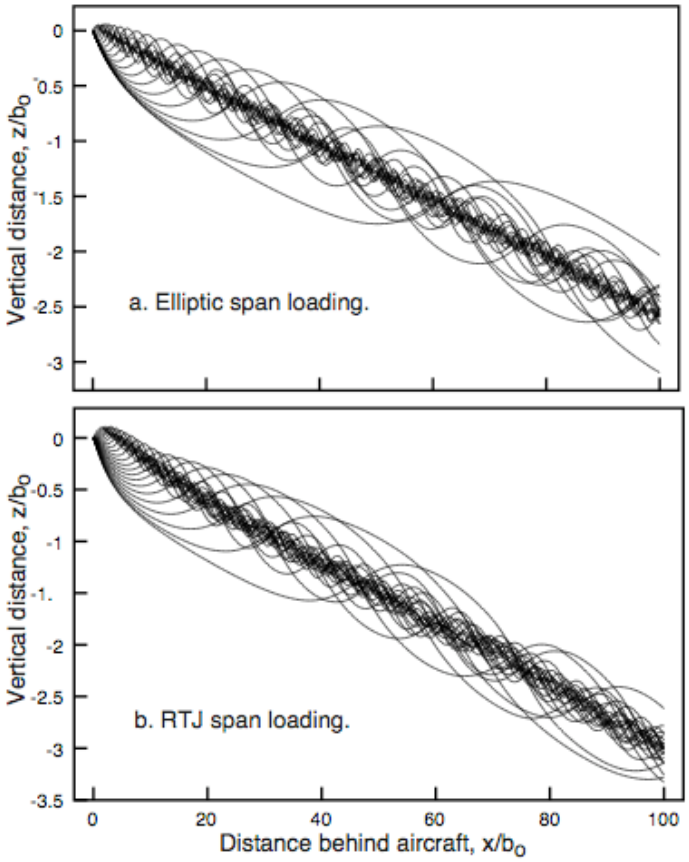


Fig. 7 Side view of the long-term roll up process of the vortex sheets shed by the two span wise loadings on a wing.

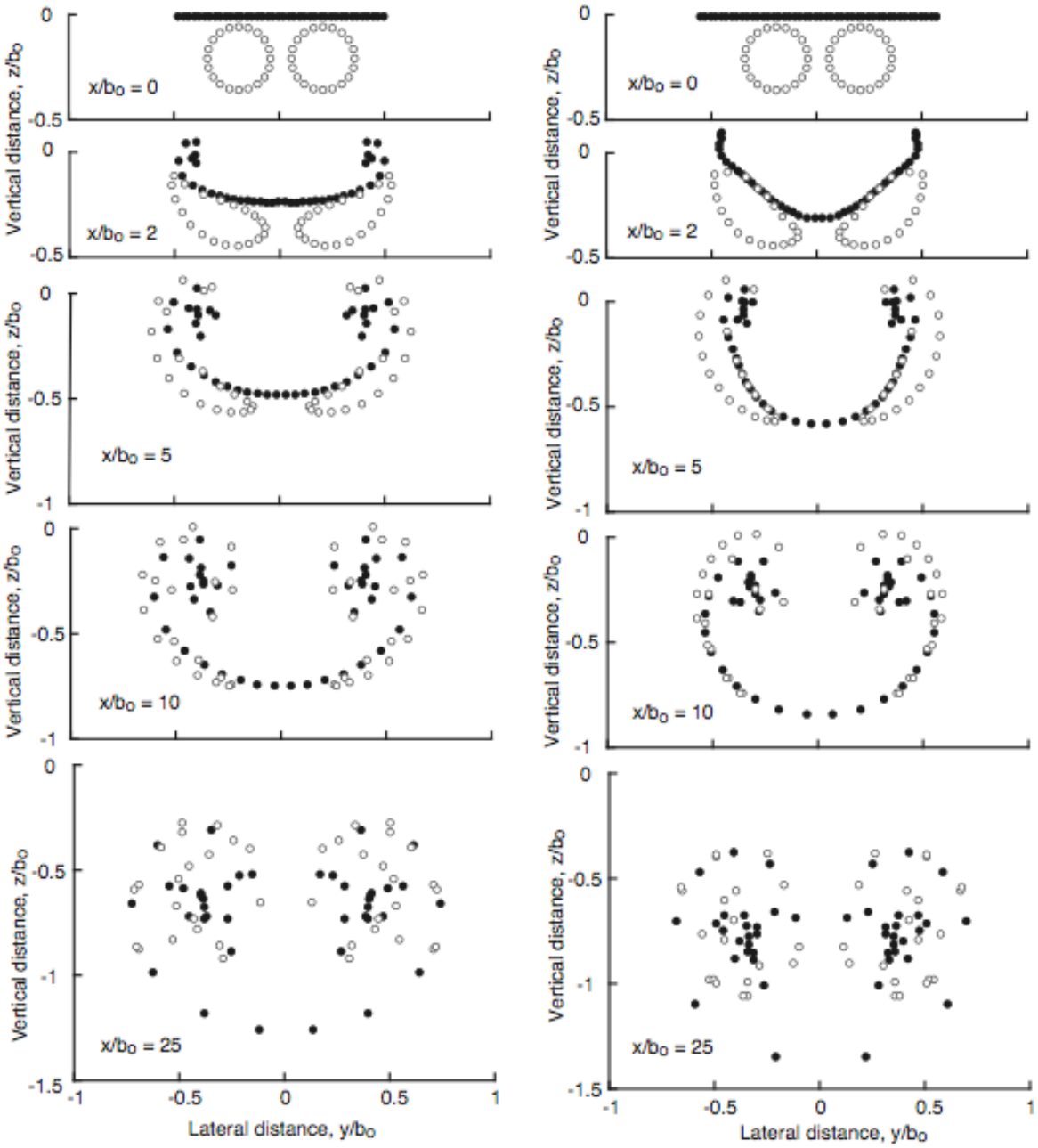


a. Elliptic span loading.

b. R. T. Jones span loading.

Fig. 8 End views of locations of point vortices ( • ) and passive fluid markers ( ○ ) at several times during history of wake dynamics for 25 span lengths.

## VI. End Views of Motion of Point Vortices with Markers.

In order to better understand the mechanisms that cause condensation trails to grow in cross-sectional size from about one span to over five spans, a sequence of cases were calculated to

determine how fluid markers mix with and move around inside wakes under the influence of vortex distributions shed by the span loadings on the two span-wise loadings being studied. For this purpose, the fluid markers are initially located around the periphery of the jet-exhaust openings for a two-engine aircraft as shown in Fig. 8 at $x/b_o = 0$. Rear views computed for both an elliptic and a R. T. Jones span loading are shown out to 25 spans behind the wake-generating wing. Because the fluid markers are benign and do not possess the characteristics of sources or vortices, they move only in response to the velocities produced by the point vortices in the flow-field. Therefore, the locations of the point vortices are not changed by the presence of the markers. The markers simply float with the local velocity field to show how exhaust jets would mix with the ambient fluid. Fig. 8 illustrates how condensate can serve as a fluid marker by mixing thoroughly with the vortex wake shed by an aircraft. The computation also shows how adjacent ambient air in the atmosphere is assimilated and mixed with the point vortices by sheet-wrapping (Fig. 3) and by convection (Fig. 8) into the flow field of the vortex pair.

## VII. Rear Views of Motion of Point Vortices with Sources.

Enlargement of the wake cross section by slowing of jet-exhaust velocities and by the assimilation of ambient air from outside of the wake are now simulated by making each marker in Fig. 8 into a point source with a strength of $m_o/2\pi b_o U_\infty = 0.05$. The open circles now represent sources in the flow field. A source strength of 0.05 was chosen as a mid-range value for the cases computed because the summation of source strengths is then 1.0 per side for elliptic loading, which is about the same magnitude as a summation of strengths for the point vortices on each side of the wake. That is, because the number of point sources and point vortices are the same in number on each side of the wake (20), the summation in strengths for both yield total strengths around 1.0 dimensionless units. If the strength chosen for the point sources was smaller or varied with time, the influence of the sources on the flow field decreased to an amount that was too small. Similarly, if the strength chosen for the point sources was larger, the influence of the sources on the flow field became unreasonably dominant. For these reasons, the strength of the sources chosen for all of the cases was the 0.05 valued indicated above.

The theoretical simulations presented indicate that the fluid added to the wakes by exhaust gases (simulated by point sources) remain near the altitude where they were generated and do not move downward nearly as fast as the vortex part of the wake, which moves downward under the self-induced velocity field of the vortices. Therefore, as wakes ages, it becomes composed of an

upper (mostly condensation) part and a lower (mostly vortex) part, as observed at cruise altitudes. Also, the point vortices also appear to group into several groups of pairs rather than spiraling around each other in a single group.

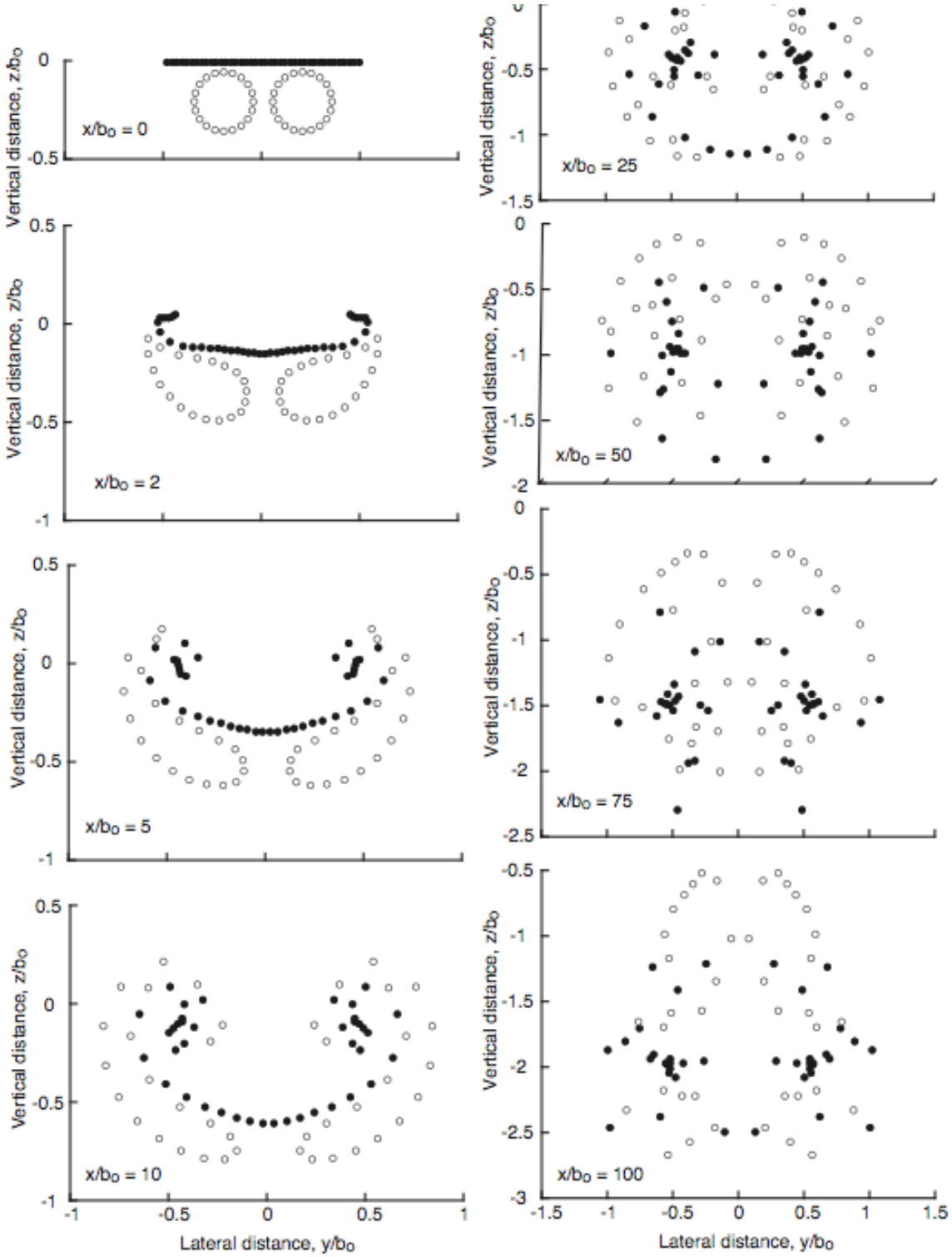


Fig. 9 Dynamics predicted for lift-generated wakes shed by elliptically-loaded wing as represented by point vortices and sources to simulate affect of exhaust products and turbulent mixing on wake structure.

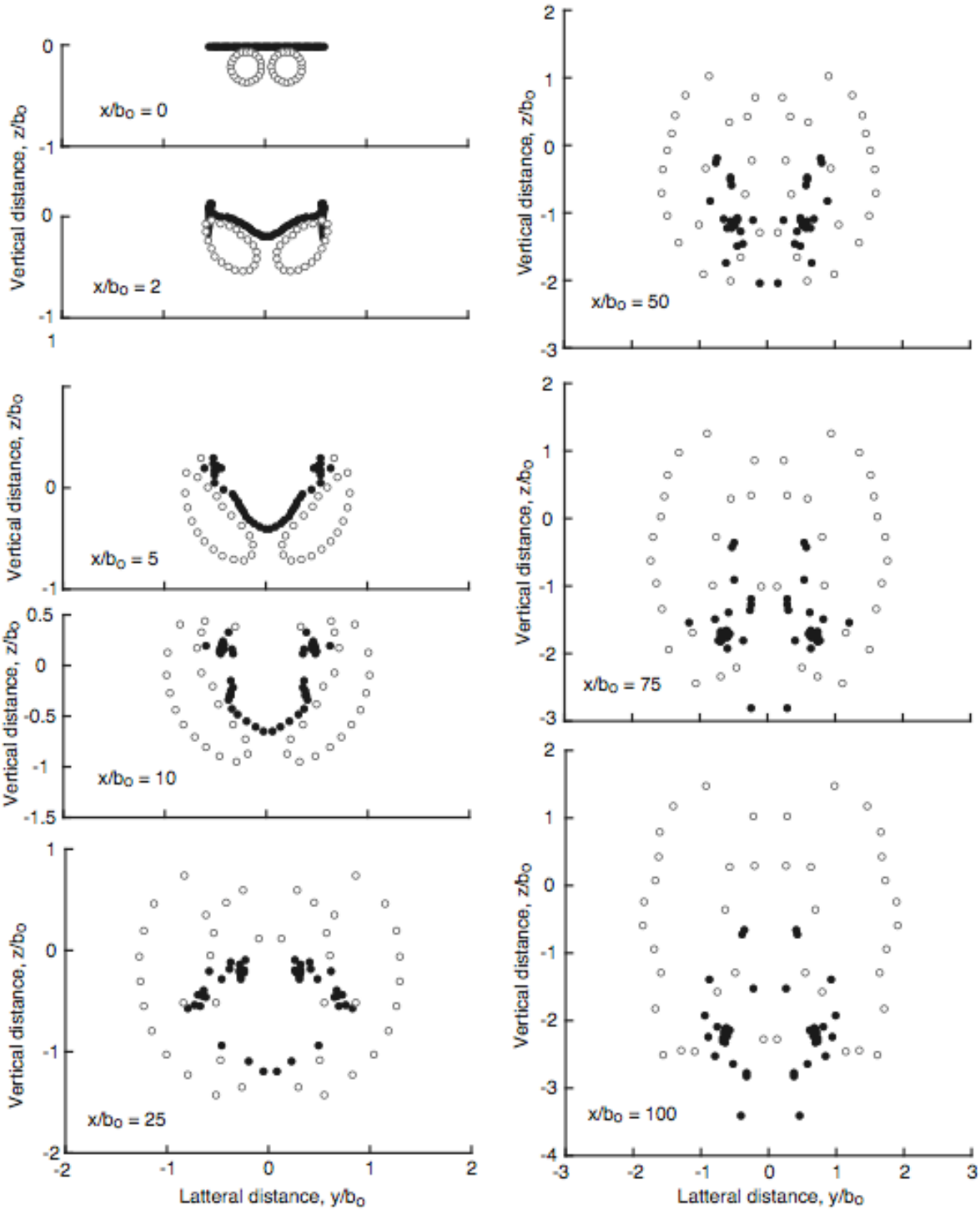


Fig. 10 Dynamics predicted for lift-generated wakes shed by wing loaded according to R. J. Jones design for minimum weight as represented by point vortices and sources to simulate affect of exhaust products and turbulent mixing on wake structure.

As shown in Figs. 9 and 10, the motion of the point sources and point vortices for both span loadings begins by moving the circular distribution of sources outboard, upward and around the wing tips. The point sources also mix with the point vortices. The emission type of flow field created by the point sources tends to push the singularities away from each other. When the point vortices move downward under their self-induced velocity field, the point sources are left behind at a higher elevations because their velocity field tends to push singularities away from each other, which does not cause the sources as a group to descend.

The RTJ loading does not mix sources and vortices as intimately as the elliptic loaded case, probably because elliptic loading has more intense vortex centers. That is, elliptic loading has its shed vorticity concentrated in its most outboard point vortices whereas the RTJ loading has the vorticity more evenly distributed across the span of the wing. This characteristic becomes more apparent as time progresses by the fact that a larger number of sources move upward and away from the vortices in the case of the RTJ loading as compared with the elliptically-loaded case. In fact, at $x/b_o = 50$, a large number of the sources have mixed with the vortices in the elliptically-loaded case and less than half have moved just outside of the main body of singularities. In the RTJ-loading case at $x/b_o = 50$, most of the sources are located on a ring well outside of the vortex distribution. This separation trend persists as time increases so that, at $x/b_o = 100$, most of the sources are located above the vortices in the RTJ case, and are quite mixed with vortices in the elliptically-loaded case. In both cases, the presence of the point sources tends to divide the single group of point vortices shed by the wing into several layers of point vortex groups.

When the flow field contains markers instead of sources (Fig. 8), the point-vortex distributions in both cases extend over and mix within the same size of area occupied by the point vortices alone; i.e., a vertical distance of about one wing span. When the sources are active, Figs. 9 and 10, the vertical extent of the point-vortex distributions at $x/b_o = 100$ extend over about 3 wing spans in the elliptically-loaded case and over more than 4 wing spans in the RTJ-loaded case. In both cases, the point vortices move downward through the source-generated fluid causing the bulk of the point vortices to be located in the lower part of the wake (in preparation for the long-wave instability). The breadth of the wake is doubled in

the elliptically-loaded case, and more than tripled in the case of the RTJ-loaded wing, which shows an effect of span loading on the rate of wake spreading, and a possible reduction in the rolling-moment hazard posed by the wake. As illustrated by the photographs in Figs. 1 and 2, onset and completion of the long-wave instability adds considerably to the further spread of the wake and condensate region.

Cases calculated for larger values of source strengths resulted in larger and more rapid separations of the wake into parts, and smaller values took longer to separate. When the source strengths were much smaller than the 0.05 value, wake separation does not occur, and the sources act only as fluid markers.

A vertical spread in the distribution of vortex pairs is suggested in Figs. 9 and 10, and in a side view of a condensation trail, Fig. 11. The clumps of condensation at the bottom of the formation are obviously the residue from the most intense part of the vortex pair that separated from the original vortex structure and migrated to the bottom of wake (Figs. 1 and 2), where the pair went through the long-wave instability. At the time of the picture, this lowest vortex pair has gone through the long-wave instability, and has formed closed loops of vortex filaments. Two other sets of vortex filaments are indicated in the upper part of the condensate by the accumulation of condensate into a dense line near the top of the condensate region, and into a line in the region about midway between the top and bottom of the condensate distribution. If so, the original single vortex sheet behind the wing appears to have had its vorticity redistributed vertically into as many as three vortical regions by mixing with ambient air and with exhaust condensate. At the time of the picture, the wake has organized itself into a form that resembles a formation of either two or three vortex-pair regions located vertically over each other. Of the three vortex pairs, the strongest is or was the lower pair which has just gone through the long-wave instability. As a result, the entire

Fig. 11 Side view of condensation trail about one and one-half minutes old showing decomposed configuration of lowest vortex pair at bottom of condensate, and core regions of two possible vortex pairs near the top and near the center of the upper part of the condensate trail.

wake has probably become benign as far as a rolling-moment hazard is concerned for in-trail encounters. However, the vertical-loads hazard posed by the wake could still be too hazardous to permit across-trail penetrations [1]. The three-vortex configuration in Fig. 11 is, of course, more conducive to decomposition than the classical single-pair configuration that forms when mixing and exhaust condensate are not present.

## VIII. Conclusions.

The computed simulations of lift-generated vortex wakes with and without exhaust condensate indicate that the presence of jet-exhaust streams in lift-generated wakes causes them to separate into two or more parts, similar to dynamics observed in condensation trails. The upper parts are composed primarily of condensate with some vorticity, and the lowest part contains the strongest parts of the vortex sheet which goes through the long-wave instability. Although the foregoing flow-field representations are approximate, they appear to simulate features frequently observed in condensation trails shed by aircraft flying at cruise altitudes. It is concluded that lift-generated vortex wakes spread more rapidly in the vertical direction when engine exhaust streams are present, than when they are absent. The calculations also indicate that the wake structures shed by different span loadings on the wake-generating wing are similar in size and shape, and have many of the same characteristics. Detailed differences are probably not important as far as wake hazard and decomposition rate are concerned.

The results presented apply to wakes of aircraft at cruise altitudes, but probably also to aircraft in their take-off and climb configurations. The results are probably not needed, however, when engines are throttled down, as for approach and landing configurations near airports. Guidelines derived previously [7,18,19] for the motion and spread of vortex wakes for aircraft on approach to an airport are then correct as derived for avoiding vortex wakes of preceding aircraft, and need not be modified. The study did not determine the effect of jet-exhaust streams on the decomposition and decay of lift-generated vortex wakes.

## IX. References

[1] Rossow, V. J., and James, K. D., "Overview of Wake-Vortex Hazards During Cruise", *AIAA Journal of Aircraft,* Vol. 37, No. 6, 2000, pp. 960-975.

[2] Brown, A. P., and Bastian, M., "Wake Vortex Core Flow Field Dynamics and Encounter Loads *In-situ* Flight Measurements", *46th AIAA Aerospace Sciences Meeting and Exhibit,* Reno, NV, 7-10 January 2008, AIAA 2008-0468.

[3] Crow, S. C., "Stability Theory for a Pair of Trailing Vortices", *AIAA Journal*, Vol. 8, No. 12, Dec. 1970, pp 2172-2179.

[4] Crow, S. C., and Bate, E. R., Jr., "Lifespan of Trailing Vortices in a Turbulent Atmosphere", *AIAA Journal of Aircraft, Vol.* 13, No. 7, July 1976, pp 476-482.

[5] Rossow, V. J., "Lift-Generated Vortex Wakes of Subsonic Transport Aircraft", *Progress in Aerospace Sciences*, Vol. 35, No. 6, Aug. 1999, pp. 507-660.

[6] Donaldson, C. duP., and Bilanin, A. J., "Vortex Wakes of Conventional Aircraft", *Advisory Group for Aerospace Research and Development*, AGARDograph No. 204, May 1975.

[7] Rossow, V. J,, and Meyn, L. A., "Guidelines for Avoiding Vortex Wakes During Use of Closely-Spaced Parallel Runways", *26th AIAA Applied Aerodynamics Conference,* Honolulu, HI, 18-21 Aug. 2008, AIAA 2008-6907.

[8] Patterson, J. C., and Jordan, F. L., Jr., "Thrust-Augmented Vortex Attenuation", Gessow, A., ed., *NASA Symposium on Wake Vortex Minimization,* NASA SP-409, 1976, pp. 251-270.

[9] Rossow, V. J., "Classical Wing Theory and the Downward Velocity of Vortex Wakes", *AIAA Journal of Aircraft*, Vol. 43, No. 2, March-April 2006, pp. 381-385.

[10] Rossow, V. J., "Extended-Betz Methods for Rollup of Vortex Sheets", *AIAA Journal of Aircraft*, Vol. 34, No. 5, Sept.-Oct, 1997, pp.592-599.

[11] Lamb, Sir Horace, *Hydrodynamics*, 6th edition, Dover, 1945, pp. 214-230.

[12] Rosenhead, L., "The Formation of Vortices from a Surface of Discontinuity," *Proceedings of the Royal Society*, London, Vol. A134, 1931, pp. 170-192.

[13] Westwater, F. L., "The Rolling Up of the Surface of Discontinuity Behind an Aerofoil of Finite Span", Aeronautical Research Council, London, Repts. and Memo. 1692, 1935, pp.116-131.

[14] Rossow, V. J., "Application of Vortex Invariants to Roll Up of Vortex Pairs", *AIAA Journal of Aircraft*, Vol. 41, No. 5, Sept.-Oct. 2004, pp. 1098-1105.

[15] Glauert, H., *The Elements of Aerofoil and Airscrew Theory*, Second Edition, Cambridge University Press, Cambridge, England, 1948, p. 155.

[16] Munk, M. M., *Fundamentals of Fluid Dynamics for Aircraft Designers*, The Ronald Press Co., New York, NY, 1929, pp. 94ff.

[17] Jones, R. T., "The Spanwise Distribution of Lift for Minimum Induced Drag of Wings Having a Given Lift and a Given Bending Moment", *NACA* Technical Note 2249, Dec. 1950; see also, "Collected Works of Robert T. Jones", *NASA* TM X-3334, Feb. 1976, pp. 539-554.

[18] Verma, S., Lozito, S., Trot, G., and Ballinger, D., "Guidelines for Flight Deck Procedures for Very Closely Spaced Parallel Runway Approaches", 27th Digital Avionics Systems Conference, October 26-30, 2008.

[19] Verma, S., Lozito, S., Trot, G., "Preliminary Guidelines on Flight Deck Procedures for Very Closely Spaced Parallel Runway Approaches", 16th International Congress of the Aeronautical Sciences, *ICAS* 2008-574-Verma-7-01-08.